

Electrochemistry in an Acoustically Levitated Drop

Edward T. Chainani, Khanh T. Ngo, Alexander Scheeline

Department of Chemistry, University of Illinois at Urbana-Champaign, 600 South Mathews
Avenue, Urbana, Illinois 61801

Microfabrication procedure. Microfabrication processes were carried out at the Beckman Institute cleanroom at the University of Illinois. Blank 3-inch silicon (<100>, N type) wafers, typically 285 μm thick (WRS Materials, San Jose, CA) were cleaned with water and solvents and baked on a hotplate at 200 $^{\circ}\text{C}$ for 5-10 min to drive off surface-bound water. HD-4100 polyimide resist (HD Microsystems, Parlin, NJ) was spin-coated onto the wafer at 5000 rpm using a Cee 200X spin coater (Brewer Science, Rolla, MO) to a film thickness of 4 μm (when cured). The resist edge-bead was removed with a spatula and post-baked according to the recommended procedure. The passivation mask was used to expose the polyimide on the Kasper 2001 aligner/exposure tool (Kasper Instruments, Mountain View, CA). This was followed by a post-exposure bake and developed using the recommended developer PA-401D and rinsed in PA-400R solutions (HD Microsystems, Parlin, NJ). The post-development bake was done at 150 $^{\circ}\text{C}$ for 100 s, followed by 200 $^{\circ}\text{C}$ for 100 s. The final cure was carried out on a hotplate (HP 61, Torrey Pines Scientific, Carlsbad, CA) with a nitrogen purge using an inverted glass funnel to keep oxygen levels below 800 ppm as required for the final cure. The recommended temperature

program was used: room temperature (RT) to 200 °C at 10 °C min⁻¹; hold 200 °C for 30 min, ramp to 375 °C at 10 °C min⁻¹; hold 375 °C for 60 min; gradual cool to RT.

To create the metal pattern, an image reversal resist is laid on the polyimide passivation prior to metal deposition. Image reversal is useful for turning a positive mask into a negative resist pattern.¹ This procedure is an alternative to metal etching, where the tendency is to have narrow lines over-etched and the wide patterns to be under-etched when both wide and narrow features are present in the design. Image reversal is useful for evaporated metal lift-off techniques, since the process results in a negative wall profile. This process retains fine (< 10 µm) features much better than etching a pattern protected by a positive resist. Prior to the use of the lift-off procedure, photoresist patterning followed by metal etching was the procedure used. Poor adhesion of the resist caused undesired etching of metal, and undercutting cause failure of adhesion of metal to substrate.

Polyimide-passivated substrates are cleaned with solvent, then water, and then subjected to O₂ plasma using a Plasmod system (Nordson-MARCH, Concord, CA) for 100 watts, 30 s. The wafer is baked at 180 °C for 2 min to remove water layer, then cooled to room temperature in a nitrogen atmosphere. An adhesion promoter was made by dissolving 1 g diphenylsilanediol (Sigma-Aldrich, St. Louis, MO) in 200 ml SU-8 developer (MicroChem, Newton, MA) and the resulting solution is spin-coated at 6000 rpm for 60 s and post baked at 180 °C for 2 min. After cooling to room temperature, AZ 5214E image reversal resist (AZ Electronic Materials, Branchburg, NJ) is spin-coated at 4000 rpm for 30 sec. After softbaking for 1 min at 95 °C, the resist is exposed using the positive image mask for a total of 19 mJ cm⁻², followed by post exposure bake for 2 min at 120 °C. This temperature is critical for image reversal, as it has to be 5° to 10 °C below the thermal cross-linking temperature. This is followed by flood exposure,

using no mask, at a dose $> 1000 \text{ mJ cm}^{-2}$, which makes the unexposed areas from the image exposure soluble. The pattern is developed with AZ 400 K (AZ Electronic Materials, Branchburg, NJ), diluted 1:5 with distilled water for 60-90 s. The wafer is rinsed with distilled water, dried with nitrogen, and inspected under a microscope. After bake-out for 1 min at 95°C and O_2 plasma 100W for 30 s, the wafer is ready for metal deposition. Metal deposition was carried out on a Temescal e-beam evaporator, at a vacuum $< 5 \times 10^{-6}$ torr. An initial 6 nm Ti adhesion layer is followed by 100 nm Au layer, with an additional 6 nm Ti adhesion layer over the gold.

Lift-off procedure is carried out by first soaking the wafer in acetone followed by 180 sec ultrasonication. This is done twice to remove large lift-off areas. Inspection under a microscope reveals if the lift-off process has been completed. If not, additional lift-off is done using 1165 Microposit remover (Shipley Co., Marlborough, MA), made up of N-methyl-2-pyrrolidone or NMP, instead of acetone. Ultrasonication in 1165 remover for 10 min breaks up the lift-off metal into tiny particles and does not harm the cured polyimide. 1165 remover may be heated to 80°C (no higher as the flash point of Microposit 1165 is 85°C) using the hotplate inside a fume hood to hasten the process. The wafer is rinsed with isopropanol (electronic grade, Fisher Scientific, Pittsburgh, PA).

The metal layer is then covered with a polyimide layer that is spin-coated, patterned and developed, and cured in much the same way as the initial polyimide passivation layer described above.

An additional layer of thick photoresist was found necessary in protecting the electrode areas from being covered or marred by debris from the laser cutting process. A $10 \mu\text{m}$ layer of AZ P4620 photoresist (AZ Electronic Materials, Branchburg, NJ) was spin-coated at 2500 rpm for

60 s. Softbaking at 110 °C 180 s was followed by cooling to room temperature, then exposure with the debris protection layer pattern at a dose of 1500-1700 mJ cm⁻². The pattern was developed using AZ 400K diluted with deionized water, 1:4, at immersion time of 60 s at room temperature. The wafer was rinsed with deionized water, dried and placed on a 110 °C hotplate for five minutes. The wafer was inspected after every process step using a Zeiss Axioscope A1. Images were acquired with a Zeiss AxioCam ICc3 color CCD camera using AxioVision LE software (Carl Zeiss, Inc., NY, USA). A calibration slide (MicroBrightField, Inc., Chicago, USA) with both 250 µm and 25 µm grid was used to set the image scale for 2.5x, 10x and 20x microscope objectives.

Individual electrodes were separated from the wafer by laser cutting (Nd:YAG, 1.06 µm, Potomac Laser, Lanham, MD, operated by University of Illinois SCS Machine Shop). The score lines required 80 passes while the central area in the vicinity of tips, which are cut through completely, required 300 passes for the 3-inch wafer (thickness about 285 µm).

After the laser cutting procedure, the wafer is thoroughly washed with water and isopropanol. Areas of wafer in the tip area should be dislodged right after the laser cutting procedure. Otherwise, a gentle spray of water will free them while leaving the narrow tips intact. Soaking the wafer with undiluted AZ 400K for 20 min strips the debris protection layer as well as any debris that have become embedded in it. The wafer is then rinsed with water and solvents and dried with a nitrogen gun. If the presence of organic residue on the metal areas is suspected, oxygen plasma etching is carried out on the wafer. The resulting wafer is shown in Figure S-1.

The individual sensors can be removed from the wafer by carefully placing the wafer on a cleanroom wipe or glass slide on a flat surface, with the edge of the wipe or slide along the score line and applying pressure on each side of the line until a clean break occurs. This is best done in

a manner that causes the wafer to break into halves, then, each half can be further subdivided into quarters, and so on. Because the laser-scored lines did not extend to the wafer edge, it was necessary to use a diamond tipped scribe and ruler to manually extend the score lines. In retrospect, the laser could have been made to score the lines to the wafer edge, because the 285 μm -thick wafer would be able to endure handling without break apart prematurely when taken off the laser mill. A similar procedure was attempted on thinner (80 μm) wafers, but these proved to be too fragile to undergo the non-automated fabrication process, breaking at the slightest opportunity.

To prevent wicking of the drop into the body of the electrode, a hydrophobic fluoropolymer (CYTOP type M, Asahi Glass Co., Ltd., Tokyo, Japan) was applied on the inactive portion of the electrode with a brush. CYTOP type M has isocyanate end functional groups that react directly with silicon surface hydroxyl groups, avoiding the need for surface activation prior to coating. However, the electrode area itself must remain uncoated to allow for contact with the solution. Beyond half a millimeter from the tip, the rest of the body is CYTOP coated. To achieve this, the electrode areas are temporarily protected by the solid lauric acid (Sigma-Aldrich, St. Louis, MO), which can be easily removed after CYTOP coating: Lauric acid was melted in a small glass dish at 50 °C and the amount of liquid adjusted so that the depth was slightly less than needed to completely submerge the tip. The sensor tip was dipped into the melted lauric acid and withdrawn to cool and solidify. CYTOP is applied by brush, with the electrode area temporarily protected by solid lauric acid. After the CYTOP dried, rinsing with isopropyl alcohol completely removed the lauric acid, and the CYTOP was cured overnight by placing the electrode in a vacuum oven at 115 °C. This procedure results in an adherent CYTOP coating that remains bonded even when the sensor is repeatedly cleaned by ultrasonication.

The Ti layer over the gold was removed by soaking the tip and the pad areas in Ti etchant (TFT, Transene Corp., Danvers MA) while sonicating. Sonication was deemed necessary for the etchant to reach the small recessed areas of the working, counter and reference electrodes. Figure S-2 shows the resulting microelectrode with integrated counter, working and reference electrodes.

Drop Geometry and Evaporation. The levitated drop acquires the approximate steady-state shape of an oblate spheroid from the balance between the acoustic, gravitational, capillary and hydrostatic forces acting on it.² In effect, the acoustic pressure “flattens” the unperturbed sphere that a drop would normally assume in the absence of acoustic forces. The oblate spheroid is a rotationally symmetric ellipsoid having a polar axis shorter than the equatorial axis. Defining the equatorial radius a and polar radius c , the volume of such a spheroid, is given by:

$$V_{os} = \frac{4}{3}\pi a^2 c \quad (\text{S-1})$$

By obtaining the lengths of the polar and equatorial axis from the camera images, the volume of the drop may be calculated from the formula above. The aspect ratio as defined in Yarin, et al.² is the ratio of equatorial to polar lengths. The surface area of an oblate spheroid is:

$$S_{os} = 2\pi a^2 \left(1 + \frac{c/a}{\sqrt{(a/c)^2 - 1}} \operatorname{arcsinh} \sqrt{(a/c)^2 - 1} \right) \quad (\text{S-2})$$

Because the evaporation of a liquid is mainly controlled by diffusion of vapor from its surface, the surface area is relevant to the rate of evaporation of the levitated drop. The evaporation of a drop of volatile liquid in still air, expressed as a change of surface area with time, is given by:³

$$\frac{dS}{dt} = \frac{8\pi DM}{R\rho} \left(\frac{P_\infty}{T_\infty} - \frac{P_d}{T_d} \right) \quad (\text{S-3})$$

where R is the gas constant, M is the gram molecular weight of the liquid, D is the vapor diffusivity in the surrounding gas of the liquid species, and ρ is the density of the liquid, P and T

are the saturation vapor pressure and temperature. The subscripts d and ∞ specify values at the drop surface and in the gas well away from the drop. If the liquid and vapor attain equilibrium, the equation above suggests that the rate is constant, such that a plot of surface area and time is linear. The surface area of a sphere $S = 4\pi r^2$ is contained in the above expression. Eq S-3 has been demonstrated experimentally to hold true for spherical levitated drops³, and seems to hold true even for spheroid drops in an acoustic field, as our data, shown in Figure S-7, suggests. Tian and Apfel⁴ used a model that shows a linear decrease of drop diameter squared over time. This would be strictly true of a spherical drop, as the surface area is a function of the square of the radius. The inset in Figure S-7 shows the evolution of the equatorial and polar diameter with time, and it can be seen that while equatorial diameter decreases with a linear trend, the change in polar diameter is nonlinear. The change of surface area with evaporation of the drop levitating about the electrode can be obtained from these data, which in this case is $-1.74 \times 10^{-2} \text{ mm}^2 \text{ sec}^{-1}$ ($r^2=0.9987$) under the conditions of relative humidity RH = 52.1%, air temperature $T = 23.5^\circ\text{C}$, and atmospheric pressure $P = 986.3 \text{ mbar}$.

In an intense sound field, acoustic streaming can be generated and the resulting convection contributes to evaporation. The exact delineation of “intense” is dependent on many factors, but, for water, it seems that sound pressure levels (SPL) $>165 \text{ dB}$ is intense enough to cause a deviation from the theoretical evaporation rate.⁵ Below 150 dB SPL , for ethanol droplets, the acoustic field offers no perturbation to the droplet evaporation process.⁴ Since we used the minimum power required for levitation, and maintained this power constant throughout the experiment, we simply assume either an insignificant or a small constant contribution of acoustic streaming to evaporation.

The rate of evaporation is critical to accurately determine drop volume, and thus analyte concentration. While the surface area loss is linear, the same cannot be said for volume. Figure S-8 shows a plot of drop *volume* against time from the same experiment shown in Figure S-7. The volume was calculated from the equatorial and polar axes obtained from the camera images, using the spheroid formula. The parameters obtained from modeling volume loss using linear and quadratic fits are tabulated in Table S-1. These parameters were used in the succeeding experiments to correct analyte concentration for evaporation.



Figure S-1. Patterned sensors on a 3-inch diameter silicon wafer. The laser-trimmed tips and the laser score lines are visible. The wafer thickness is 285 μm .

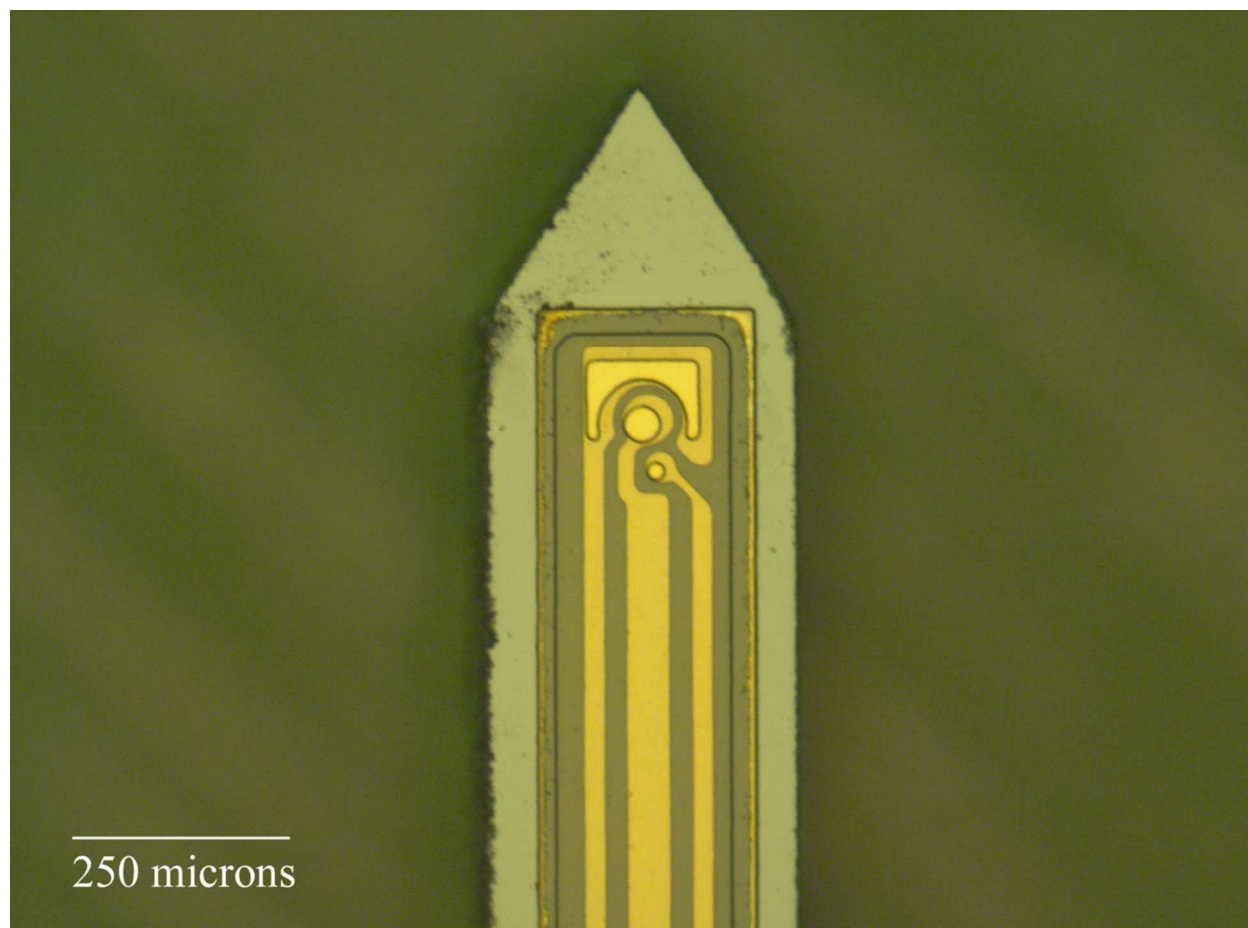


Figure S-2. Microelectrode fabricated from silicon wafer and laser-trimmed. This microscope picture of the tip shows the counter, working and reference electrodes. Woo-Hyuck Choi is acknowledged for suggesting the electrode geometry incorporated here.

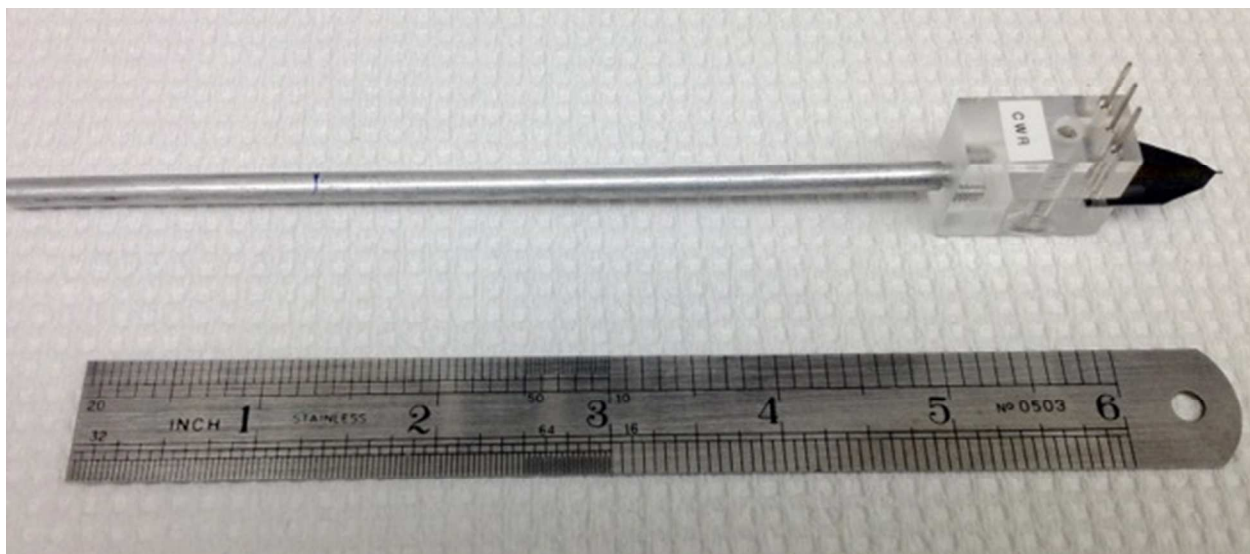


Figure S-3. Microelectrode held in a custom-built holder with spring-loaded electrical contacts.

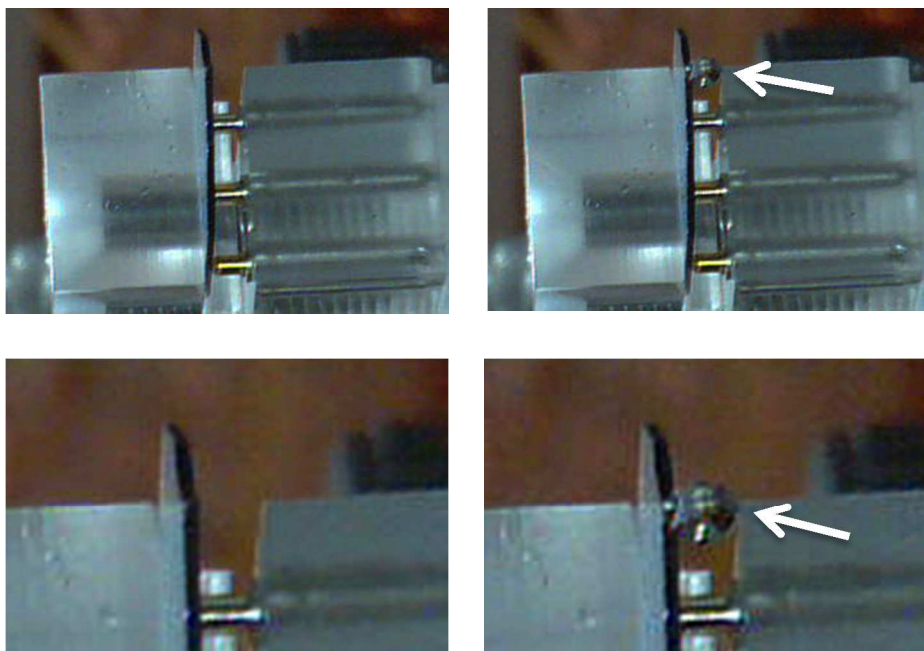


Figure S-4. Photograph of electrode taken along the longitudinal axis (top left) showing the position of the drop, marked with arrows, during levitation (top right). Bottom pictures show enlargements of the pictures on top.



Figure S-5. Photographs of the electrode positioned in the resonant cavity. From left to right: A) Electrode without a drop, showing region of tip which is CYTOP-polymer coated. B) Electrode with pendant drop. C) Electrode with acoustically levitated drop.

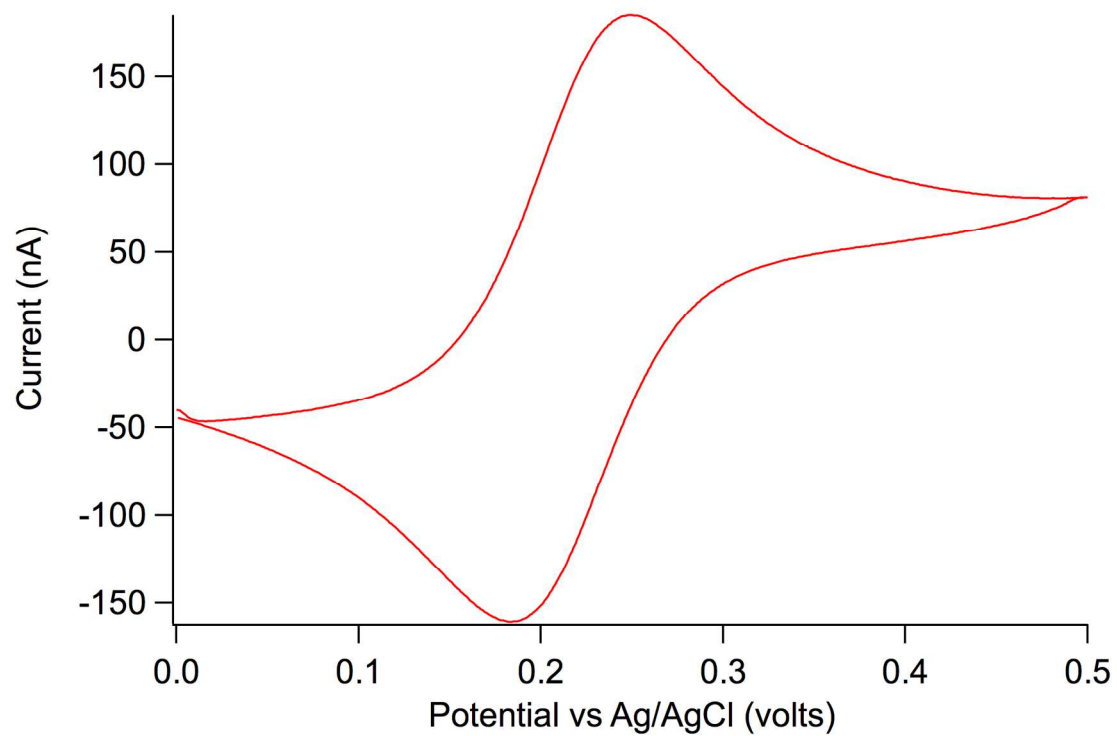


Figure S-6. Background-subtracted CV (0.1 V s^{-1}) of 0.3 mM ferrocenemethanol in 0.1 M sodium phosphate buffer taken using 1 mm radius gold electrode. Taken for comparison with behavior of microdisk microfabricated electrode.

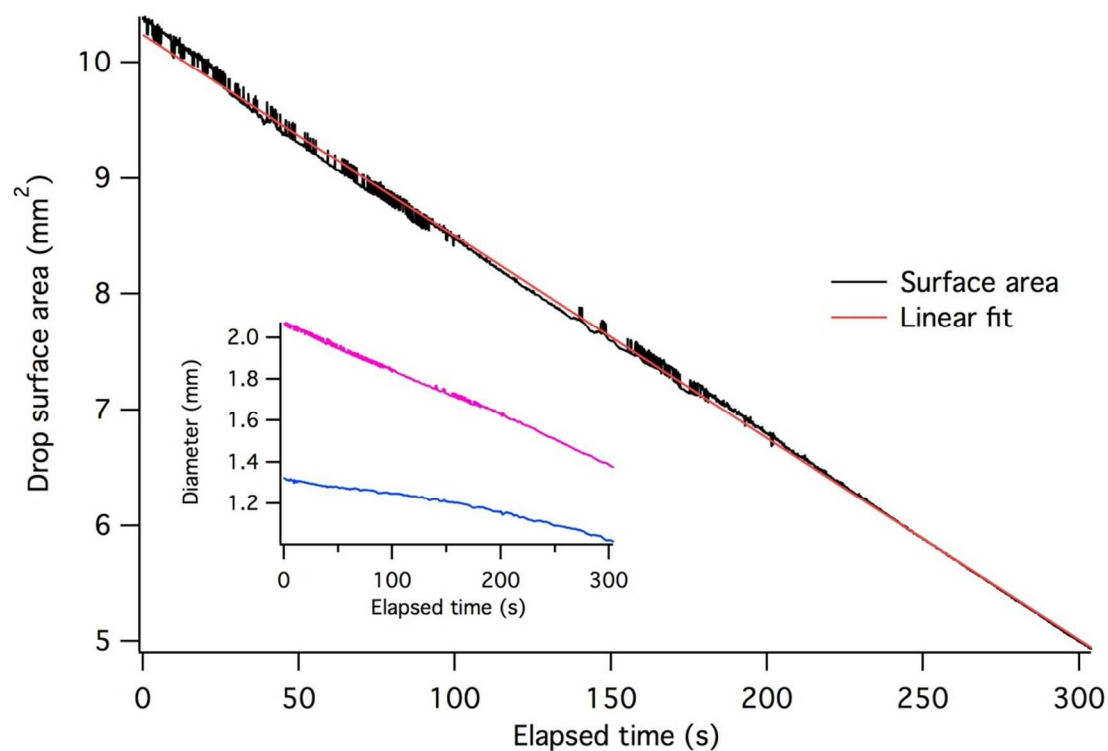


Figure S-7. Plot of drop surface area vs. time. The drop is levitated on an electrode. RH = 52.1%, T = 23.5 °C, P = 986.3 mbar. The inset shows the evolution of the equatorial (magenta) and polar (blue) diameters over time. The source of the noise spikes is mainly the equatorial diameter data (see inset). Spikes seen in the equatorial diameter data are largely absent in the polar diameter data, most likely due to the greater orbital vs. axial motion (with consequent image blur). Drop motion is more restricted along the polar axis due to the spatial structure of the acoustic standing wave.

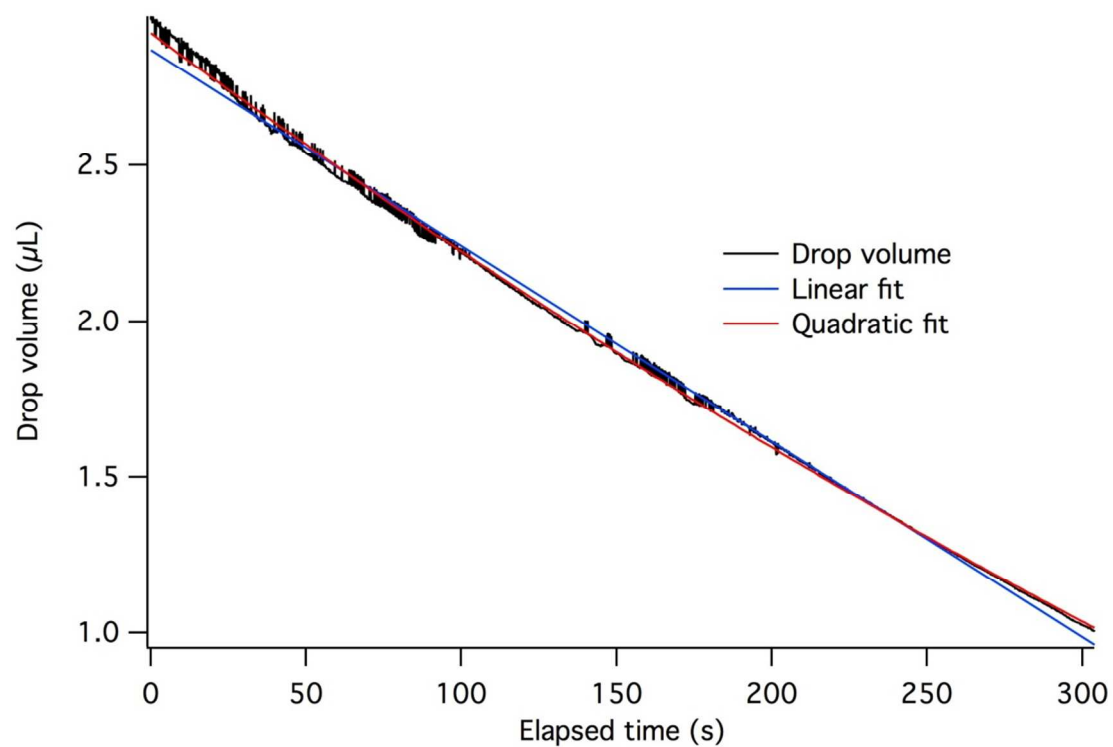


Figure S-8. Plot of drop volume vs. time, with the same conditions as Figure S-7. A linear (blue) and a quadratic fit (red) are superimposed over the data points (black).

Table S-1. Fit parameters for drop volume to determine the rate of evaporation (in $\mu\text{l s}^{-1}$) of a levitated drop positioned on the microelectrode.

Linear		Quadratic	
<i>Parameter</i>	<i>Value</i>	<i>Parameter</i>	<i>Value</i>
intercept (μl)	2.87	a_0 (μl)	2.93
slope ($\mu\text{l s}^{-1}$)	$-6.28 \cdot 10^{-3}$	a_1 ($\mu\text{l s}^{-1}$)	$-7.34 \cdot 10^{-3}$
		a_2 ($\mu\text{l s}^{-2}$)	$3.47 \cdot 10^{-6}$

References

- (1) Madou, M. J., *Fundamentals of microfabrication: the science of miniaturization*, CRC Press, Boca Raton, Fla., **2002**, p. 723.
- (2) Yarin, A. L.; Pfaffenlehner, M. and Tropea, C. *J.Fluid Mech.* **1998**, 356, 65.
- (3) Seaver, M.; Galloway, A. and Manuccia, T. J. *Rev.Sci.Instrum.* **1989**, 60, 3452.
- (4) Tian, Y. and Apfel, R. E. *J.Aerosol Sci.* **1996**, 27, 721.
- (5) Yarin, A. L.; Brenn, G.; Kastner, O.; Rensink, D. and Tropea, C. *J.Fluid Mech.* **1999**, 399, 151.